DOI: 10.1002/adsc.201300786

Structural Determinants for the Non-Canonical Substrate Specificity of the ω-Transaminase from *Paracoccus denitrificans*

Eul-Soo Park,[+a] Sae-Rom Park,[+a] Sang-Woo Han,[a] Joo-Young Dong,[a] and Jong-Shik Shin[a,*]

[a] Department of Biotechnology, Yonsei University, Shinchon-Dong 134, Seodaemun-Gu, Seoul 120-749, South Korea
Fax: (+82)-2-362-7265; phone: (+82)-2-2123-5884; e-mail: enzymo@yonsei.ac.kr

[+] E.-S. Park and S.-R. Park equally contributed to the work.

Received: September 6, 2013; Published online: January 8, 2014

Supporting information for this article is available on the WWW under http://dx.doi.org/10.1002/adsc.201300786.

Abstract: Substrate binding pockets of ω-transaminase (ω-TA) consist of a large (L) pocket capable of dual recognition of hydrophobic and carboxyl substituents, and a small (S) pocket displaying a strict steric constraint that permits entry of a substituent no larger than an ethyl group. Despite the unique catalytic utility of ω-TA enabling asymmetric reductive amination of carbonyl compounds, the severe size exclusion occurring in the S pocket has limited synthetic applications of ω-TA to access structurally diverse chiral amines and amino acids. Here we report the first example of an ω-TA whose S pocket shows a non-canonical steric constraint and readily accommodates up to an *n*-butyl substituent. The relaxed substrate specificity of the (*S*)-selective ω-TA, cloned from *Paracoccus denitrificans* (PDTA), afforded efficient asymmetric syntheses of unnatural amino acids carrying long alkyl side chains such as L-norvaline and L-norleucine. Molecular modeling using the recently released X-ray structure of PDTA could pinpoint an exact location of the S pocket which had remained dubious. Entry of a hydrophobic substituent in the L pocket was found to have the S pocket accept up to an ethyl substituent, reminiscent of the canonical steric constraint. In contrast, binding of a carboxyl group to the L pocket induced a slight movement of V153 away from the small-pocket-forming residues. The resulting structural change elicited excavation of the S pocket, leading to formation of a narrow tunnel-like structure allowing accommodation of linear alkyl groups of carboxylate-bearing substrates. To verify the active site model, we introduced site-directed mutagenesis to six active site residues and examined whether the point mutations alleviated the steric constraint in the S pocket. Consistent with the molecular modeling results, the V153A variant assumed an elongated S pocket and accepted even an *n*-hexyl substituent. Our findings provide precise structural information on substrate binding to the active site of ω-TA, which is expected to benefit rational redesign of substrate specificity of ω-TA.

Keywords: active site; asymmetric amination; site-directed mutagenesis; substrate specificity; ω-transaminase

Introduction

ω-Transaminase (ω-TA) mediates the stereoselective amino group transfer between an amino donor and an acceptor using pyridoxal 5′-phosphate (PLP) as a prosthetic group.[1] The broad substrate specificity of the enzyme enables oxidative deamination of primary amines and amino acids as well as reductive amination of ketones, keto acids and aldehydes.[1c–f] This unique catalytic property of ω-TA, executable without the aid of an external cofactor, has prompted recent research efforts to harness the enzyme as a powerful synthetic toolkit for asymmetric synthesis of enantiopure amines and amino acids from achiral carbonyl precursors.[1c–f,2]

Substrate specificities of more than forty ω-TAs identified to date, including both (*S*)- and (*R*)-selective ones, turned out to share key features which could be explained by an empirical two-binding-site model consisting of a large (L) and a small (S) pocket (Scheme 1).[1c,e,3] The L pocket displays a dual recognition mode that allows accommodation of a hydrophobic substituent (Scheme 1A) as well as a carboxylate (Scheme 1B), reminiscent of aspartate transaminase

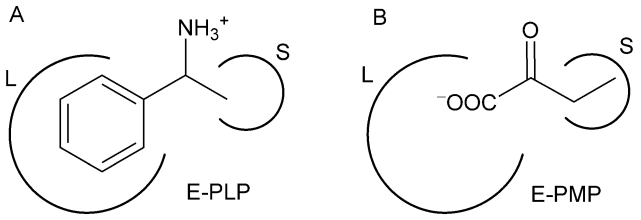

Scheme 1. The two-binding-site model of ω-TA. A) Binding of α-methylbenzylamine to a PLP form of the enzyme (E-PLP). B) Binding of 2-oxobutyrate to a pyridoxamine 5′-phosphate form of the enzyme (E-PMP).

and aromatic amino acid transaminase.[1a,4] The S pocket is characterized by a strict steric constraint that allows entry of substituents only up to an ethyl group (Scheme 1B). Indeed, no naturally occurring ω-TA has been reported to be able to readily accept a substituent bulkier than an ethyl group in the S pocket.[1c,e] The two-binding-site model has successfully explained observed substrate spectrum of ω-TAs, which underlies canonical substrate specificity of the enzyme.

In the context of asymmetric synthesis of structurally diverse chiral amines[5] and amino acids[6] which are important chiral building blocks of various pharmaceuticals, the severe steric constraint in the S pocket seriously limits the product range accessible by the ω-TA approach.[7] To cope with this limitation, one could use either protein engineering to excavate the S pocket of naturally occurring enzymes[2b,8] or public database searching to discover a new enzyme showing a desirable substrate specificity.[9] The former option was successfully implemented to create a variant of (*R*)-selective ω-TA from *Arthrobacter* sp. capable of accepting bulky substituents of aryl alkyl ketones used for asymmetric synthesis of chiral amines.[2b]

In this report, we aim at addressing following questions. First, is there a naturally occurring ω-TA that disobeys the canonical steric constraint in the S pocket? Second, where is the exact location of the S pocket and which residues serve as a steric barrier responsible for rejecting bulky substituents? In the previous study, we identified and cloned (*S*)-selective ω-TAs from *Ochrobactrum anthropi* (OATA) and *Paracoccus denitrificans* (PDTA) by public database searching.[2c,10] We fortuitously found that PDTA could readily aminate 2-oxopentanoate as efficiently as it did pyruvate. This finding led us to explore whether PDTA is the first example of ω-TA that deviates from the canonical steric constraint.

Results and Discussion

Comparison of Amino Acceptor Reactivities

To scrutinize the difference in the steric constraints of the S pockets of OATA and PDTA, we set out to compare amino acceptor reactivities of α-keto acids carrying structurally diverse alkyl substituents that served as probes to assess the steric constraint (Table 1). As expected, the S pocket of OATA showed the canonical steric constraint not allowing entry of a substituent larger than an ethyl group. Compared with glyoxylate (**1a**) and pyruvate (**1b**), 2-oxobutyrate (**1c**) showed a drastic decrease in the amino acceptor reactivity and eventually relative reactivities less than 1% were detected with α-keto acids carrying substituents bulkier than an ethyl group (i.e., **1d–1i**). In contrast, PDTA showed a markedly relaxed steric constraint that enabled high reactivities of α-keto acids carrying linear alkyl substituents even up to an *n*-butyl group [i.e., 2-oxohexanoate (**1f**)]. To our surprise, 2-oxooctanoate (**1i**) carrying an *n*-hexyl substituent displayed even 3% reactivity relative to **1b**. However, contrary to the α-keto acids carrying linear alkyl substituents, PDTA did not show any activity toward branched-chain α-keto acids (**1e**, **1g–1h**). Taken together, the S pocket of PDTA showed a relaxed steric constraint toward linear alkyl substituents which is distinct from canonical ω-TAs such as OATA.

Table 1. Amino acceptor specificities of OATA and PDTA toward α-keto acids carrying alkyl side chains.

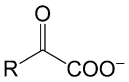	R	Relative reactivity[a] [%]	
		OATA	PDTA
1a	-H	129 ± 7	103 ± 6
1b	-CH_3	100 ± 4	100 ± 3
1c	-CH_2CH_3	14 ± 2	82 ± 7
1d	-$(CH_2)_2CH_3$	n.r.[b]	105 ± 3
1e	-$CH(CH_3)_2$	n.r.	n.r.
1f	-$(CH_2)_3CH_3$	n.r.	77 ± 8
1g	-$CH(CH_3)CH_2CH_3$	n.r.	n.r.
1h	-$C(CH_3)_3$	n.r.	n.r.
1i	-$(CH_2)_5CH_3$	n.r.	3 ± 1

[a] Relative reactivity represents the initial reaction rate (i.e., conversion < 10%) normalized by that of **1b**. Reaction conditions to measure the initial rates were α-keto acid (10 mM) and (*S*)-α-methylbenzylamine (20 mM) in 50 mM phosphate buffer (pH 7.0) at 37 °C.

[b] n.r.: not reactive (i.e., relative reactivity < 1%).

Table 2. Amino donor specificities of OATA and PDTA toward L-α-amino acids carrying alkyl side chains.

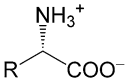

	R	Relative reactivity[a] [%]	
		OATA	PDTA
2a	-H	3±1	2±1
L-**2b**	-CH_3	100±5	100±6
L-**2c**	-CH_2CH_3	7±1	37±3
L-**2d**	-$(CH_2)_2CH_3$	n.r.[b]	81±2
L-**2e**	-$CH(CH_3)_2$	n.r.	n.r.
L-**2f**	-$(CH_2)_3CH_3$	n.r.	23±4
L-**2g**	-$CH(CH_3)CH_2CH_3$	n.r.	n.r.
L-**2h**	-$C(CH_3)_3$	n.r.	n.r.
L-**2i**	-$(CH_2)_5CH_3$	n.r.	n.r.

[a] Relative reactivity represents the initial reaction rate normalized by that of L-**2b**. Reaction conditions were propanal (20 mM) and L-α-amino acid [20 mM; except L-**2i** (1 mM) owing to the low solubility (≈1.6 mM)].
[b] n.r.: not reactive (i.e., relative reactivity <1%).

Table 3. Amino donor specificities of OATA and PDTA toward (*S*)-α-methylbenzylamine and its analogues.

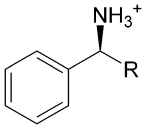

	R	Relative reactivity[a] [%]	
		OATA	PDTA
(*S*)-**3a**	-CH_3	100±2	100±3
(*S*)-**3b**	-CH_2CH_3	7±1	14±3
(*S*)-**3c**	-$(CH_2)_2CH_3$	n.r.[b]	5±2
(*S*)-**3d**[c]	-$CH(CH_3)_2$	n.r.	n.r.
(*S*)-**3e**[c]	-$C(CH_3)_3$	n.r.	n.r.

[a] Relative reactivity represents the initial reaction rate normalized by that of (*S*)-**3a**. Reaction conditions were (*S*)-amine (20 mM) and **1b** (20 mM).
[b] n.r.: not reactive (i.e., relative reactivity <1%).
[c] Racemic amine (40 mM) was used in the initial rate measurement.

Comparison of Amino Donor Reactivities

To confirm the relaxed steric constraint in the S pocket of PDTA, we examined substrate specificity toward L-α-amino acids (Table 2). Consistent with the reactivities of α-keto acids, OATA exhibited no activities to L-α-amino acids carrying side chains bulkier than an ethyl group (i.e. L-**2d**–**2i**). In contrast, PDTA showed substantial activities toward L-norvaline (L-**2d**) and L-norleucine (L-**2f**) whose corresponding α-keto acids were reactive amino acceptors. Notably, both ω-TAs displayed very low reactivities of glycine (**2a**) relative to L-alanine (L-**2b**) despite the higher reactivity of **1a** than **1b**.

The L pocket is taken up by a carboxylate when the L-α-amino acid forms a Michaelis complex with E-PLP. To examine whether entry of a hydrophobic substituent, instead of the carboxylate, into the L pocket might influence the steric constraint in the S pocket of PDTA, we measured amino donor reactivities of (*S*)-α-methylbenzylamine [(*S*)-**3a**] and its analogues in which the methyl group of (*S*)-**3a** was substituted by bulkier alkyl groups (Table 3). As expected, OATA lacked activities to the structural analogues of (*S*)-**3a** where the alkyl substituents were larger than an ethyl group [i.e., (*S*)-**3c**–**3e**]. Intriguingly, unlike the relaxed steric constraint observed with L-α-amino acids, PDTA showed much lower relative reactivities of (*S*)-α-ethylbenzylamine [(*S*)-**3b**] and (*S*)-1-phenylbutylamine [(*S*)-**3c**] than L-**2c** and L-**2d**, respectively. This result suggests that binding of a hydrophobic substituent to the L pocket restores the steric constraint in the S pocket to a canonical state. Taken together, the type of a substituent taking up the L pocket (i.e., hydrophobic *vs.* carboxyl) seems to affect spatial arrangement of the residues forming the S pocket of PDTA.

Synthetic Utility of the Non-Canonical Substrate Specificity

To demonstrate exploitation of the relaxed steric constraint of PDTA, we carried out asymmetric syntheses of unnatural amino acids from α-keto acids bearing a substituent bulkier than an ethyl group. To this end, isopropylamine (IPA) was chosen as an amino donor owing to its cheap price and the high volatility of a resulting deamination product (i.e., acetone).[2b,e,11] In the previous study, amino donor reactivity of IPA relative to (*S*)-**3a** was 7 and 43% measured with PDTA and OATA, respectively.[12] To illustrate the synthetic utility of PDTA over OATA, we carried out transamination between **1f** and IPA using the two ω-TAs (Figure 1A). PDTA afforded conversion higher than 99% at 4 h. Enantiomeric excess (*ee*) of the produced L-**2f** was >99%. In contrast, very low activity of OATA toward **1f** (i.e., less than 1% of **1b**) led to only 10% conversion after 4 h despite the much higher relative reactivity of IPA.

For the semi-preparative scale synthesis of unnatural amino acids, we performed syntheses of L-**2d** and L-**2f** from the corresponding α-keto acids (100 mM) using PDTA in 10 mL reaction mixture (Figure 1B). Owing to the higher reactivity of **1d** than **1f**, asymmetric synthesis of L-**2d** proceeded faster than that of L-**2f**. After 100 min, conversions of both reactions reached >99% and the enantiopurities of the resulting L-amino acids were > 99% *ee*.

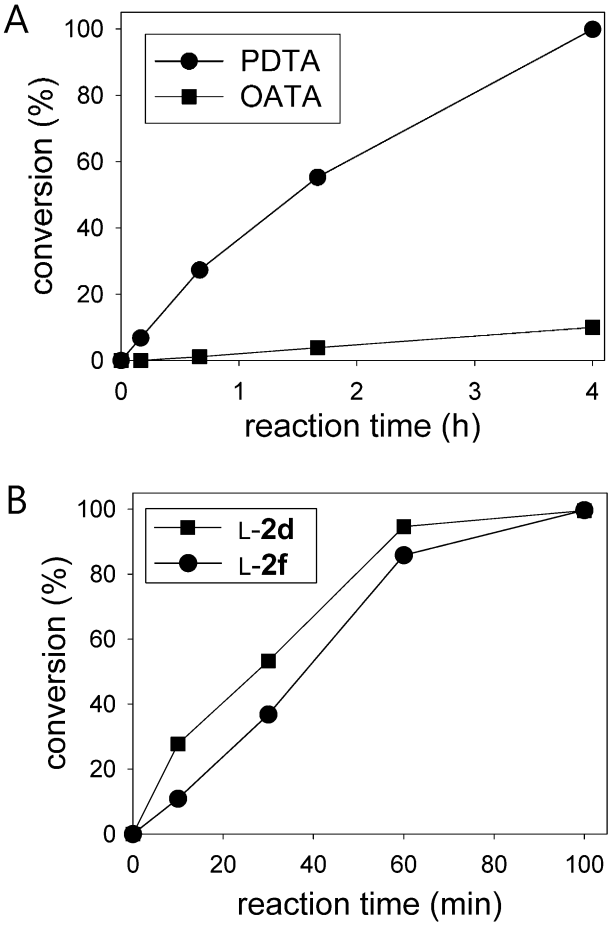

Figure 1. Asymmetric synthesis of unnatural amino acids from α-keto acids and IPA. A) Conversion of **1f** with L-**2f** using PDTA and OATA. Reaction conditions were **1f** (20 mM), IPA (50 mM) and ω-TA (4 μM). B) Semi-preparative synthesis of L-**2d** and L-**2f** using PDTA. Reaction conditions were α-keto acids (100 mM), IPA (200 mM) and PDTA (40 μM) in 10 mL reaction mixture.

Molecular Modeling of the Substrate Binding

We previously proposed a two-binding-site model of ω-TA based on active site mapping using structurally diverse substrates.[3] The active site model has been in accordance with available X-ray structures of ω-TAs.[9b,13] However, in contrast to the L pocket readily noticeable in the active site, the exact location of the S pocket remained unclear. This was due to a failure in obtaining a reliable docking model of arylalkylamines, such as (*S*)-**3a**, within the active site where an active site Arg, responsible for recognition of a carboxylate, protrudes into the L pocket and thereby interferes with the phenyl group of (*S*)-**3a**.[10] The inward-facing conformation of the active site Arg was exclusively observed in the X-ray structures of both subunits of the ω-TAs from *Pseudomonas putida* (PDB ID: 3A8U),[13a] *Vibrio fluvialis* (3NUI)[13d] and *Chromobacterium violaceum* (4A6T).[13b]

To provide a structural basis for the relaxed steric constraint in the S pocket of PDTA, we performed molecular modeling using the recently published X-ray structure of homodimeric PDTA (PBD ID: 4GRX).[13e] Although overall structures of the two subunits were very similar (root-mean-square deviation of backbone atoms = 0.59 Å), the active site R415 showed a significant conformational difference in the two subunits (Figure 2A). The side chain of R415 points away from the active site in the subunit A owing to the presence of a substrate analogue (i.e., 5-aminopentanoate) bound to the active site. The outward-facing conformation of the active site Arg was also recently observed with other ω-TAs (PDB ID: 3HMU and 3FCR).[9b] In contrast, R415 in the subunit B adopts an inward-facing conformation and consequently restricts the L pocket.

We conjectured that the active sites of the subunit A and B adopted structural arrangements competent for binding to substrates carrying a hydrophobic and a carboxyl group, respectively. Accordingly, we first carried out docking of (*S*)-**3a** in the active site of the subunit A using the Discovery Studio package (Figure 2B). The phenyl group of (*S*)-**3a** was tightly packed in the L pocket where five aromatic amino acids, that is, F19, W57, F85*, F86* and Y150, were located proximally to the phenyl group and thereby provided hydrophobic environments. Note that the asterisks in F85* and F86* mean that the residues come from the other subunit. The methyl group of (*S*)-**3a** pointed toward a shallow pit which was surrounded by F19, F85*, Y150, V153, F321* and a phosphate group of the internal aldimine, formed between PLP and K285. Molecular modeling shows that alkyl substituents only up to an ethyl group fit in this pit [see Figure S1 in the Supporting Information for a docking model of (*S*)-**3b**], which is in agreement with the experimental results. Therefore, the modeling results clearly indicate that the shallow pit serves as the S pocket.

Substrate specificity studies performed with α-keto acids and L-α-amino acids indicated that the steric constraint in the S pocket was remarkably relaxed when the L pocket was bound to a carboxylate. Indeed, molecular modeling showed that the S pocket in the subunit B assumed a deep narrow pit capable of accepting up to an *n*-butyl group of L-**2f** (Figure 2C). Due to the extended structure, the S pocket forms additional contacts with the side chains of S118 and F321*. The inward-facing R415 enables formation of multiple hydrogen bonds with the α-carboxylate of L-**2f**. The energetic gain coming from the H-bond formation seems to drive the amino group of L-**2f** to be positioned close to the C-4′ of the PLP moiety, which is an essential spatial requirement for subsequent catalytic conversion to an external aldimine. The same spatial requirement of the amino group of (*S*)-**3a**, as

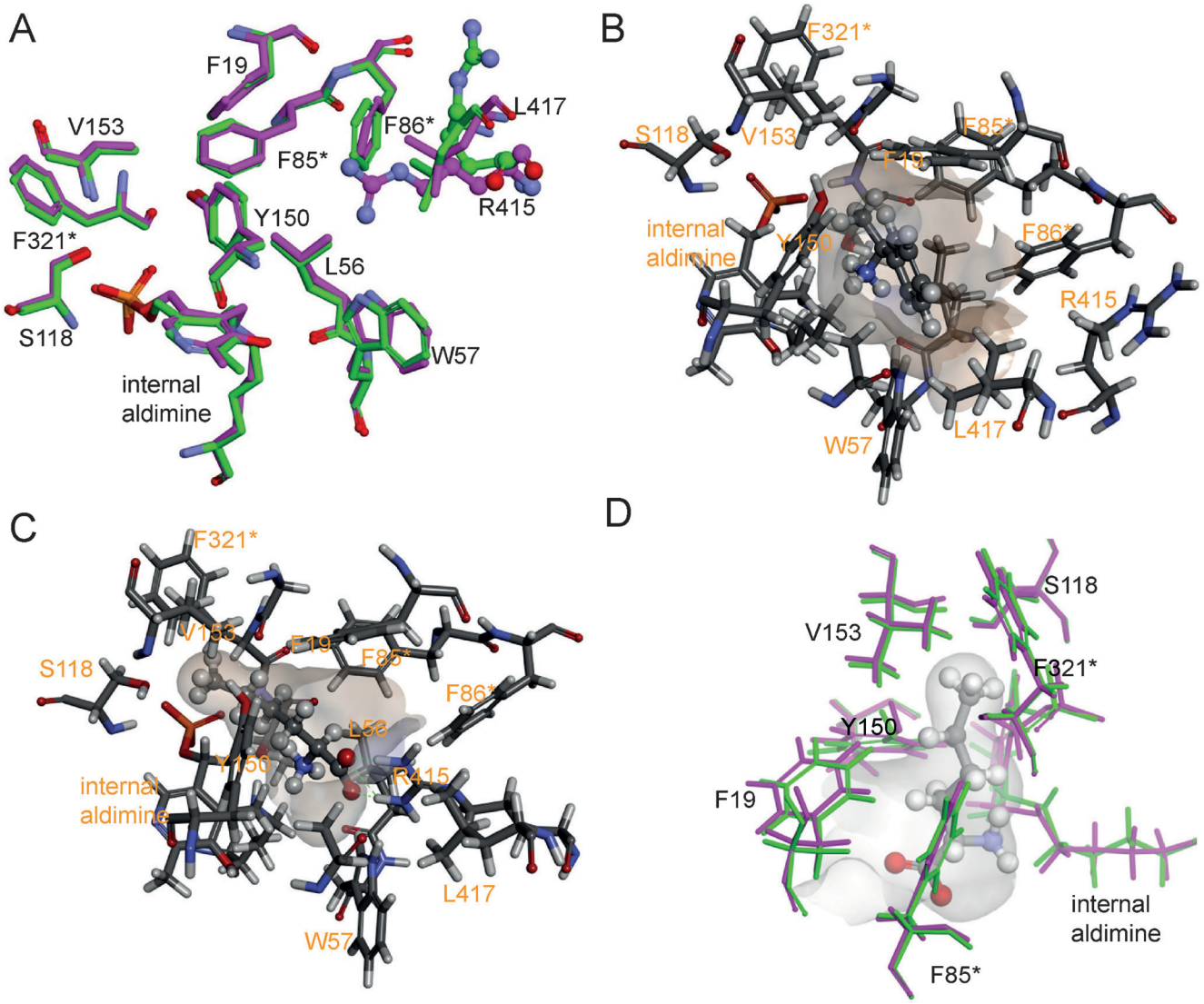

Figure 2. Molecular modeling of the active site of PDTA. A) Structural alignment of the key active site residues in subunit A and B, colored in green and magenta, respectively. R415 is shown in a ball-and-stick representation. B) Docking of (*S*)-**3a** (shown as a ball-and-stick model) in subunit A. C) Docking of L-**2f** (shown as a ball-and-stick model) in subunit B. Green dotted lines represent hydrogen bonds between the carboxylate of L-**2f** and the guanidinium group of R415. D) Structural alignment of the small-pocket-forming residues in subunit A (colored in green) onto the docking model of L-**2f** in subunit B (colored in magenta).

shown in Figure 2B, seems to be driven by the tight packing of the phenyl group in the hydrophobic L pocket, owing to the structural transition of R415 into an outward-facing conformation.

To identify amino acid residues that act as a conformational switch controlling the shape of the S pocket, structural alignment of the five relevant residues and the internal aldimine was performed (Figure 2D). We found that V153 was the only residue that moved back from the S pocket in the subunit B. In contrast to the slight movement of V153 beneficial for the S pocket extension, other residues and the internal aldimine did not make such a contribution. Therefore, V153 seems to play a key role in discriminating the subtle difference in the bulkiness of substituents entering the S pocket, depending on the type of a substituent bound to the L pocket.

Structure-Guided Engineering of the S Pocket

Based on the molecular modeling results, we could pinpoint the exact location of the S pocket and reveal the structural basis for the non-canonical substrate specificity of PDTA. To verify these findings, we carried out alanine scanning mutagenesis of six active site residues (i.e., F19, L56, F85*, Y150, V153 and L417) and examined whether the point mutations into

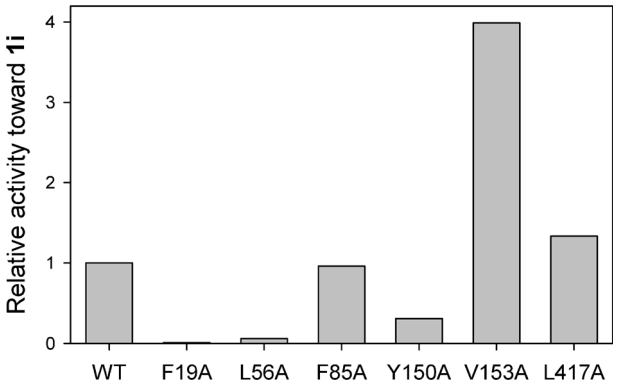

Figure 3. Alanine scanning mutagenesis to identify a residue involved in the steric constraint in the S pocket. Relative activity represents the initial reaction rate of the alanine mutant normalized by that of the wild-type PDTA. Reaction conditions were **1i** (10 mM), (*S*)-**3a** (10 mM) and ω-TA (0.2 μM). Initial rate for the wild-type enzyme was 20 μM min^{-1}.

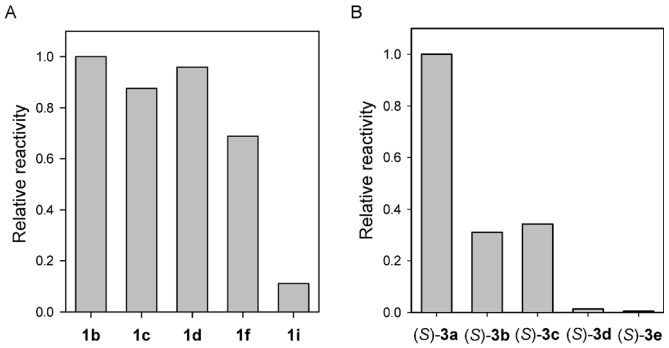

Figure 5. Substrate specificity of the V153A variant. A) Reactivities of α-keto acids carrying linear alkyl side chains. *Reaction conditions:* α-keto acids (10 mM), (*S*)-**3a** (10 mM) and ω-TA (0.1 μM). B) Reactivities of (*S*)-**3a** and its analogues. *Reaction conditions:* **1b** (10 mM), (*S*)-amine (10 mM) and ω-TA (0.1 μM). Initial rate measured at 10 mM **1b** and 10 mM (*S*)-**3a** was 375 μM min^{-1}.

a much smaller amino acid enhanced enzyme activity toward **1i** carrying an *n*-hexyl substituent. Among the six mutations, only V153A permitted an increase in the reactivity of **1i** compared with the wild-type PDTA (Figure 3). The four-fold activity enhancement of the V153A mutant relative to the wild-type enzyme is in agreement with the molecular modeling results indicating that V153 would be a conformational switch to the structural alteration of the S pocket.

To visualize how the V153A mutation led to a higher activity toward the substrate carrying an *n*-hexyl substituent, we performed docking simulations of L-**2i** and the V153A variant (Figure 4). We found that L-**2i** formed productive binding to the active site of subunit B (i.e., proximal orientations of the carboxyl and the amino group of L-**2i** to the guanidinium group of R415 and C-4′ of the PLP, respectively) without a steric clash between the linear alkyl side chain and the small-pocket-forming residues. In contrast, V153 present in the wild-type enzyme engendered steric clashes with the terminus of the *n*-hexyl group.

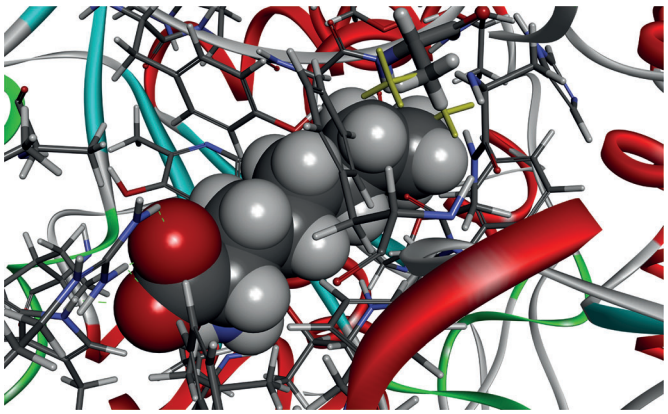

Figure 4. Docking of L-**2i** in the subunit B of the V153A variant. L-**2i** is shown as a CPK model where red and blue hemispheres represent oxygen and nitrogen atoms, respectively. Green dotted lines represent hydrogen bonds between the carboxylate of L-**2i** and the R415. Thin yellow and thick grey sticks represent the original V153 and its alanine mutation, respectively.

To examine whether the excavation of the S pocket induced by the V153A mutation promotes accommodation of alkyl chains shorter than a *n*-hexyl group, we measured activities of the V153A variant toward α-keto acids carrying linear alkyl substituents of varying lengths (Figure 5A). Taken together with Table 1, the V153A mutation did not affect relative reactivities of **1c**, **1d** and **1f**, carrying side chains that were readily accepted by the wild-type S pocket, but improved reactivity of **1i**. This result indicates that entry of alkyl substituents, from ethyl to *n*-butyl groups, in the S pocket does not undergo steric hindrance and thereby excavation of the S pocket did not elicit reactivity enhancement.

Compared with the subunit B, the S pocket in the subunit A is sterically more restricted by the slight protrusion of V153 toward the S pocket. Therefore, it was expected that the V153A variant might exhibit enhanced reactivities of arylalkylamines carrying alkyl substituents bulkier than an ethyl group. Indeed, the V153A variant showed 34% relative activity toward (*S*)-**3c**, compared with (*S*)-**3a** (Figure 5B). However, the reactivity enhancement was not observed with (*S*)-**3a** analogues carrying branched alkyl substituents [i.e., (*S*)-**3d** and **3e**]. Taken together, the mutational study corroborates the molecular modeling results revealing that V153 controls accessibility of bulky substituents in the S pocket by a slight move-

ment in response to the type of a substituent bound to the L pocket.

Conclusions

In this study, we report the first example of a naturally occurring ω-TA that can readily accept substituents bulkier than an ethyl group in the S pocket. The relaxed steric constraint in the S pocket confers non-canonical substrate specificity on PDTA, which affords extension of a product pipeline accessible by ω-TAs. Molecular simulations enabled us to identify the exact location of the S pocket and to reveal that V153 of PDTA serves as a molecular switch controlling the S pocket structure which is determined by a substituent type taking up the L pocket. This structural information was successfully exploited for engineering of the S pocket to accept bulky substituents even up to an *n*-hexyl group, otherwise up to an *n*-butyl group. We expect that these findings may facilitate active site engineering to create an ω-TA variant that can accommodate structurally diverse substrates.

Experimental Section

Chemicals

1b and **1h** were obtained from Kanto Chemical Co. (Tokyo, Japan) and Tokyo Chemical Industry Co. (Tokyo, Japan), respectively. L-**2b** was purchased from Acros Organics (Geel, Belgium). L-**2e** and L-**2g** were purchased from Samchun Chemical Co. (Seoul, South Korea) and Daejung Chemical & Metals Co. (Siheung, South Korea), respectively. (*S*)-**3c** was purchased from Alfa Aesar (Ward Hill, USA). *rac*-**3d** and *rac*-**3e** were purchased from Enamine Ltd. (Kiev, Ukraine). Isopropylamine (IPA) was purchased from Junsei Chemical Co. (Tokyo, Japan). All other chemicals were purchased from Sigma Aldrich Co. (St. Louis, USA) and were of the highest grade available.

Preparation of Purified ω-TA

Overexpression and purification of OATA, PDTA and variants of PDTA were carried out as described previously with a few modifications.[2c,10] *Escherichia coli* BL21 (DE3) cells transformed with the pET28a(+) expression vector harboring the ω-TA gene were cultivated in LB medium containing 50 $\mu g\,mL^{-1}$ kanamycin at 37 °C. Protein expression was induced by IPTG around 0.6 OD_{600} and then the cells were allowed to grow further for 10 h. The culture broth was centrifuged and the resulting cell pellet was resuspended in resuspension buffer (50 mM Tris-HCl at pH 7, 50 mM NaCl, 1 mM EDTA, 1 mM β-mercaptoethanol, 0.1 mM PMSF and 0.5 mM PLP). The cells were disrupted by an ultrasonic disruptor and then centrifuged to remove cell debris.

Enzyme purification was carried out on an ÄKTAprime plus (GE Healthcare, USA). The cell-free extract was loaded on a HisTrap HP column (GE Healthcare) to purify the His_6-tagged ω-TA and eluted using an elution buffer (20 mM sodium phosphate, 0.5 M sodium chloride, 0.5 mM PLP, pH 7.4) with a linear gradient of imidazole. Buffer exchange of the purified enzyme solution was carried out by a HiTrap desalting column (GE Healthcare) using an elution buffer (50 mM sodium phosphate, 0.15 M sodium chloride and 0.5 mM PLP). When necessary, the purified enzyme solution was concentrated by an ultrafiltration kit (Ultracel-30) purchased from Millipore Co. (Billerica, USA).

Site-Directed Mutagenesis

Six variants of PDTA carrying a point mutation into alanine were created by a QuikChange Lightning site-directed mutagenesis kit (Stratagene) according to an instruction manual. Mutagenesis primers, shown in Table S1 in the Supporting Information, were designed using a primer design program (http://www.stratagene.com). The template used for the mutagenesis PCR was pET28-pdTA which was previously constructed.[2c] Intended mutagenesis was confirmed by DNA sequencing.

Enzyme Assay

Unless otherwise specified, enzyme assays were carried out at 37 °C and pH 7 (50 mM potassium phosphate buffer). Typical reaction volume was 200 μL and the reaction was stopped by adding 75 μL of 16% (v/v) perchloric acid after 10 min reaction. One unit of ω-TA activity was defined as the enzyme amount catalyzing the formation of 1 μmole of acetophenone in 1 min at 10 mM (*S*)-**3a** and 10 mM **1b**.

Substrate Specificity

To examine substrate specificity, initial reaction rates were measured. Conversions were less than 10% in the initial rate measurements which were independently triplicated. Reaction conditions to measure amino acceptor reactivities were 10 mM α-keto acid and 20 mM (*S*)-**3a** in 50 mM phosphate buffer (pH 7.0) at 37 °C. For PDTA variants, concentration of (*S*)-**3a** was 10 mM. Produced acetophenone was analyzed by HPLC.

To measure amino donor reactivities of L-α-amino acids, amino donor (20 mM) and propanal (20 mM) were used as substrates and the α-keto acids produced were analyzed by HPLC. Final concentration of L-**2i** used in the reaction mixture was 1 mM due to the low solubility. To measure amino donor reactivities of (*S*)-amines, amino donor (20 mM) and **1b** (20 mM) were used and a ketone product was analyzed by HPLC. In the case of (*S*)-**3d** and **3e**, produced L-**2b** was analyzed due to the commercial unavailability of the ketone products. Racemic **3d** and **3e** (40 mM) were used in the reactions due to the commercial unavailability of the (*S*)-enantiomers. For PDTA variants, 10 mM (*S*)-amine [except (*S*)-**3d** and **3e**; 20 mM racemic amine) and 10 mM **1b** were used.

Asymmetric Synthesis of Unnatural Amino Acids

To compare the reaction progresses of asymmetric amination of **1f** using OATA and PDTA, reaction conditions were

20 mM **1f**, 50 mM IPA, 0.5 mM PLP, 4 μM ω-TA and 50 mM phosphate buffer (pH 7) in 0.5 mL reaction mixture.

For semi-preparative synthesis of L-**2d** and L-**2f** using PDTA, reaction conditions were 100 mM α-keto acids (**1d** or **1f**), 200 mM IPA, 0.5 mM PLP, 40 μM PDTA and 50 mM phosphate buffer (pH 7) in 10 mL reaction mixture.

Conversions were measured by analyzing residual α-keto acid substrate by HPLC. Enantiomeric excess of the amino acid product was measured by HPLC.

Analytical Methods

HPLC analyses were performed with a Waters HPLC system (Waters, USA) or an YL9300 HPLC system (YL Instrument Co., South Korea). Quantitative analyses of α-keto acids and ketones using an Aminex HPX-87H column (Bio-Rad, USA) and a Sunfire C18 HPLC column (Waters, USA), respectively, were carried out as described elsewhere.[2c] Chiral analyses of **2d** and **2f** were performed by HPLC after derivatization with Marfey's reagent as described elsewhere.[14] Determination of the analyte concentrations was carried out using calibration curves obtained with authentic samples. Details of the HPLC analyses are described in the Supporting Information.

Molecular Modeling

All molecular modeling studies were performed with the Discovery Studio package (version 3.5.0, Accelrys, USA) using the CHARMM force field. Docking simulations of (*S*)-**3a** were carried out using the CDOCKER module within the active site of the subunit A identified by the Binding-Site module. The CDOCKER module was run at a default setting (heating step: 700 K and 2,000 steps; cooling step: 300 K and 5,000 steps; grid extension: 8 Å).

In the case of L-**2b**, the aforementioned docking procedures failed to generate a substrate pose assuming the productive binding in the active site of the subunit B. Therefore, L-**2b** was initially positioned in the active site with the productive binding mode fulfilled (i.e., proximal orientations of the carboxyl and the amino group of L-**2b** to the guanidinium group of R415 and C-4′ of the PLP, respectively). Energy minimization of the manually positioned L-**2b** was performed with only the substrate allowed to move until the RMS gradient reached 0.1 kcal mol^{-1} Å. The methyl group of the energy-minimized conformation of L-**2b** pointed toward the same S pocket as the methyl group of (*S*)-**3a** did. To obtain the docking model of L-**2f**, the methyl group of L-**2b** was modified to an *n*-butyl group and then energy minimization of L-**2f** was carried out.

The active site model of the V153A variant was created by substituting V153 with alanine and then by energy-minimizing the alanine moiety. To obtain the docking model of L-**2i**, the docking model of L-**2f** obtained with the wild-type PDTA was modified to L-**2i** and then energy minimization of the resulting L-**2i** was performed within the active site of the V153A variant.

Acknowledgements

This work was supported by the Advanced Biomass R&D Center (ABC-2011-0031358) through the National Research Foundation of Korea funded by the Ministry of Education, Science and Technology.

References

[1] a) K. Hirotsu, M. Goto, A. Okamoto, I. Miyahara, *Chem. Rec.* **2005**, *5*, 160–172; b) B. Y. Hwang, B. K. Cho, H. Yun, K. Koteshwar, B. G. Kim, *J. Mol. Catal. B: Enzym.* **2005**, *37*, 47–55; c) D. Koszelewski, K. Tauber, K. Faber, W. Kroutil, *Trends Biotechnol.* **2010**, *28*, 324–332; d) M. Höhne, U. T. Bornscheuer, *ChemCatChem* **2009**, *1*, 42–51; e) M. S. Malik, E. S. Park, J. S. Shin, *Appl. Microbiol. Biotechnol.* **2012**, *94*, 1163–1171; f) S. Mathew, H. Yun, *ACS Catal.* **2012**, *2*, 993–1001.

[2] a) D. Koszeleivski, I. Lavandera, D. Clay, G. M. Guebitz, D. Rozzell, W. Kroutil, *Angew. Chem.* **2008**, *120*, 9477–9480; *Angew. Chem. Int. Ed.* **2008**, *47*, 9337–9340; b) C. K. Savile, J. M. Janey, E. C. Mundorff, J. C. Moore, S. Tam, W. R. Jarvis, J. C. Colbeck, A. Krebber, F. J. Fleitz, J. Brands, P. N. Devine, G. W. Huisman, G. J. Hughes, *Science* **2010**, *329*, 305–309; c) E. Park, M. Kim, J. S. Shin, *Adv. Synth. Catal.* **2010**, *352*, 3391–3398; d) M. Höhne, S. Kühl, K. Robins, U. T. Bornscheuer, *ChemBioChem* **2008**, *9*, 363–365; e) K. E. Cassimjee, C. Branneby, V. Abedi, A. Wells, P. Berglund, *Chem. Commun.* **2010**, *46*, 5569–5571.

[3] J. S. Shin, B. G. Kim, *J. Org. Chem.* **2002**, *67*, 2848–2853.

[4] V. N. Malashkevich, J. J. Onuffer, J. F. Kirsch, J. N. Jansonius, *Nature Struct. Biol.* **1995**, *2*, 548–553.

[5] a) T. C. Nugent, *Chiral Amine Synthesis: Methods, Developments and Applications*, Wiley-VCH, Weinheim, **2010**; b) M. Breuer, K. Ditrich, T. Habicher, B. Hauer, M. Kesseler, R. Sturmer, T. Zelinski, *Angew. Chem.* **2004**, *116*, 806–843; *Angew. Chem. Int. Ed.* **2004**, *43*, 788–824.

[6] a) J. S. Ma, *Chimica Oggi* **2003**, *21*, 65–68; b) M. Breuer, K. Ditrich, T. Habicher, B. Hauer, M. Keßeler, R. Stürmer, T. Zelinski, *Angew. Chem.* **2004**, *116*, 806–843; *Angew. Chem. Int. Ed.* **2004**, *43*, 788–824; c) A. S. Bommarius, M. Schwarm, K. Drauz, *Chimia* **2001**, *55*, 50–59; d) S. Servi, D. Tessaro, G. Pedrocchi-Fantoni, *Coord. Chem. Rev.* **2008**, *252*, 715–726.

[7] E.-S. Park, J.-Y. Dong, J.-S. Shin, *ChemCatChem* DOI:10.1002/cctc.201300571, in press.

[8] U. T. Bornscheuer, G. W. Huisman, R. J. Kazlauskas, S. Lutz, J. C. Moore, K. Robins, *Nature* **2012**, *484*, 185–194.

[9] a) M. Höhne, S. Schätzle, H. Jochens, K. Robins, U. T. Bornscheuer, *Nature Chem. Biol.* **2010**, *6*, 807–813; b) F. Steffen-Munsberg, C. Vickers, A. Thontowi, S. Schätzle, T. Tumlirsch, M. S. Humble, H. Land, P. Berglund, U. T. Bornscheuer, M. Höhne, *ChemCatChem* **2013**, *5*, 150–153.

[10] E.-S. Park, M. Kim, J.-S. Shin, *Appl. Microbiol. Biotechnol.* **2012**, *93*, 2425–2435.

[11] a) M. E. B. Smith, B. H. Chen, E. G. Hibbert, U. Kaulmann, K. Smithies, J. L. Galman, F. Baganz, P. A. Dalby, H. C. Hailes, G. J. Lye, J. M. Ward, J. M. Woodley, M. Micheletti, *Org. Process Res. Dev.* **2010**, *14*, 99–107; b) F. G. Mutti, C. S. Fuchs, D. Pressnitz, J. H. Sattler, W. Kroutil, *Adv. Synth. Catal.* **2011**, *353*, 3227–3233.
[12] E.-S. Park, J.-Y. Dong, J.-S. Shin, *Org. Biomol. Chem.* **2013**, *11*, 6929–6933.
[13] a) N. Watanabe, K. Sakabe, N. Sakabe, T. Higashi, K. Sasaki, S. Aibara, Y. Morita, K. Yonaha, S. Toyama, H. Fukutani, *J. Biochem.* **1989**, *105*, 1–3; b) M. S. Humble, K. E. Cassimjee, M. Hãkansson, Y. R. Kimbung, B. Walse, V. Abedi, H. J. Federsel, P. Berglund, D. T. Logan, *FEBS J.* **2012**, *279*, 779–792; c) C. Sayer, M. N. Isupov, A. Westlake, J. A. Littlechild, *Acta Crystallogr. Sect. D. Biol. Crystallogr.* **2013**, *69*, 564–576; d) T. H. Jang, B. Kim, O. K. Park, J. Y. Bae, B. G. Kim, H. Yun, H. H. Park, *Acta Crystallogr. Sect. F: Struct. Biol. Cryst. Commun.* **2010**, *66*, 923–925; e) C. Rausch, A. Lerchner, A. Schiefner, A. Skerra, *Proteins: Struct., Funct., Bioinf.* **2013**, *81*, 774–787.
[14] E.-S. Park, M. S. Malik, J.-Y. Dong, J.-S. Shin, *ChemCatChem* **2013**, *5*, 1734–1738.

